The Astrophysical Journal Letters, 984:L4 (7pp), 2025 May 1 https://doi.org/10.3847/2041-8213/adc9a9

Contribution of Alfvénic Waves on the Formation and Deflection of Switchbacks: Insights from Two Decades of WIND Spacecraft Data

Hui Li[1,2,3], Fanzhuo Dai[1,2,3], Chi Wang[1,2,3], Wence Jiang[1,2,3], and Haoyu Li[1,2,3]
[1] State Key Laboratory of Space Weather, National Space Science Center, Chinese Academy of Sciences, Beijing, 100190, People's Republic of China; hli@nssc.ac.cn
[2] Key Laboratory of Solar Activity and Space Weather, National Space Science Center, Chinese Academy of Sciences, Beijing, 100190, People's Republic of China
[3] University of Chinese Academy of Sciences, Beijing, People's Republic of China
Received 2025 February 17; revised 2025 April 4; accepted 2025 April 7; published 2025 April 23

Abstract

Switchbacks, characterized by large-angle deflections of the local interplanetary magnetic field relative to the background, are frequently observed throughout the heliosphere and play a crucial role in the solar wind dynamics. Recent studies have highlighted the importance of local generation mechanisms, such as expanding waves, turbulence, velocity shear, and footpoint motion, in the formation of switchbacks. Utilizing nearly two decades of data from the WIND spacecraft near 1 au, we conducted a detailed investigation into the differences between switchbacks and their surrounding environment, focusing on the influence of solar wind conditions on their occurrence rate and deflection degree. Our findings indicate that switchbacks are embedded within Alfvén waves, and their occurrence rate and maximum deflection degree are significantly enhanced during large-amplitude Alfvén waves. Specifically, the occurrence rate of switchbacks during these periods shows no significant correlation with solar wind velocity, suggesting that Alfvén wave activity is the primary driver of switchback formation. Our results further indicate that the evolution of switchbacks is closely related to the evolution of Alfvén waves, and that velocity shear and footpoint motion do not play an additional role in their evolution. These findings provide valuable insights into the dynamics of switchbacks and their relationship with solar wind conditions, contributing to a deeper understanding of the complex interactions within the heliosphere.

Unified Astronomy Thesaurus concepts: Solar wind (1534); Interplanetary magnetic fields (824)

1. Introduction

Switchbacks, defined as large-angle deflections of the interplanetary magnetic field relative to the background direction, are prevalent features in fast and slow solar winds beyond 0.3 au. These phenomena have been observed by spacecraft such as Ulysses, Helios 1 and 2, WIND, and ACE (Y. Yamauchi et al. 2004; J. E. Borovsky 2016; T. S. Horbury et al. 2018). Notably, the Parker Solar Probe (PSP) has detected unprecedented switchbacks, particularly during its close approaches to the Sun, revealing characteristics of patchy distributions (S. Bale et al. 2019; J. C. Kasper et al. 2019). Given their potentially significant role in the generation and evolution of the solar wind, numerous mechanisms for switchback formation have been proposed, including interchange reconnection, coronal jets, expanding Alfvén waves and turbulence, velocity shear and footpoint motion (L. Fisk & J. Kasper 2020; D. Ruffolo et al. 2020; J. Squire et al. 2020; A. C. Sterling & R. L. Moore 2020; G. Zank et al. 2020; N. Schwadron & D. McComas 2021; M. Shoda et al. 2021). Statistical analyses of the occurrence rate and deflection evolution of switchbacks are essential for testing these hypotheses.

T. Dudok de Wit et al. (2020) introduced the normalized deflection angle as a quantitative measure of magnetic field deflection. Their study of PSP Encounter 1 data revealed that switchbacks are self-similar structures, lacking characteristic deflection degrees and durations. Subsequent research has employed this quantitative method to analyze satellite data from various orbits and periods.

During PSP Encounters, V. K. Jagarlamudi et al. (2023) observed an increase in the occurrence rate of switchbacks and the proportion of long-duration events with increasing heliocentric distance. Y. D. Liu et al. (2023) found that in the low-Mach boundary layer region, an ideal environment for interchange reconnection, the occurrence rate and deflection degree of switchbacks are suppressed. N. Huang et al. (2023) reported that the number of jets detected in situ by PSP per day is less than one, suggesting that jets alone cannot account for all switchback regions. W. Cheng et al. (2024) noted that the radial magnetic field is remarkably smooth in the subsonic solar wind, leading to the near disappearance of switchbacks.

At larger heliocentric distances, A. R. Macneil et al. (2020) found that the proportion of time during which the magnetic field deflects relative to the Parker spiral direction increases with the heliocentric distance. A. Tenerani et al. (2021) showed that within a time window of more than 1 hr, the occurrence rate of switchbacks increases with the heliocentric distance within 1 au. F. Pecora et al. (2022) further demonstrated that the occurrence rate per unit correlation length increases with the heliocentric distance, with the most rapid growth occurring in regions closer to the Sun.

These studies collectively suggest that in situ mechanisms are crucial for switchback formation. However, there remains a notable lack of comparative research investigating which local mechanism plays the dominant role in this process. In this Letter, we analyze nearly two decades of data from the WIND spacecraft (1994 November–2024 September) to identify switchbacks based on statistical definitions. By systematically examining how solar wind Alfvénicity and other factors

influence both the occurrence rate and deflection magnitude of switchbacks, we further demonstrate which formation mechanism might be more likely to dominate.

Section 2 describes the data set and methodology used in this study, including the identification of switchbacks and the detection of Alfvénic fluctuations. Section 3 presents the results. Section 4 gives some discussions and implications. Finally, Section 5 gives a brief summary.

2. Data Sets and Methodology

This study utilizes interplanetary magnetic field and solar wind plasma data from the WIND spacecraft, spanning the period from 1994 November to 2024 September. The data are recorded in geocentric solar ecliptic (GSE) coordinates with a temporal resolution of 3 s (R. Lepping et al. 1995; R. Lin et al. 1995). We restrict our analysis to the intervals where the satellite's position in the GSE coordinate system exceeds 20 Earth radii in the x-direction. For these periods, we identify continuous magnetic field data segments that last longer than 6 hr and have no gaps exceeding 120 s. Correspondingly, we select ion data segments that last more than 2 hr with no gaps exceeding 120 s. This selection ensures high-quality data for our analysis.

2.1. Diagnosis of Switchbacks

To identify potential switchbacks, we employ the "normalized deflection" z as defined by T. Dudok de Wit et al. (2020):

$$z(t) = \frac{1}{2}[1 - \cos\theta(t)], \tag{1}$$

where θ denotes the angle between the local and the average magnetic field within a 6 hr window as suggested in T. Dudok de Wit et al. (2020). We define a "potential switchback" as $z \geqslant 0.25$. For each event, the start time (t_S) is marked by the first point where z exceeds the threshold, while the end time (t_E) is marked by the first data point after the last exceedance. To avoid splitting events due to temporary drops in z, we merged adjacent events if the duration of the longer event exceeds the interval between them. We then recorded the maximum deflection for each merged event, selecting only those with a maximum deflection exceeding 0.5, indicating a significant reversal in the magnetic field direction.

We exclude potential heliospheric current sheet (HCS) crossings using the method described by F. Pecora et al. (2022). These crossings are identified by opposite signs in the average magnetic field component B_R or B_X (in the RTN and GSE coordinates, respectively) exceeding 3 nT in absolute value, averaged over 1 hr before and after the event.

Next, we assess the magnetic compressibility of the remaining events by calculating the ratio of the standard deviation of the total magnetic field strength within the interval $[t_S - \Delta t, t_E + \Delta t]$ to its mean, where $\Delta t = t_E - t_S$ represents the duration of the Switchback. This ratio, denoted as ($C_{\rm SB}$), is inspired by A. Tenerani et al. (2021). Events with $C_{\rm SB} \geqslant 0.1$ are excluded, as they likely represent magnetic field intensity variations rather than pure rotations. We address the implications of this criterion in the discussion section, noting that some studies do not apply this distinction (A. R. Macneil et al. 2020; F. S. Mozer et al. 2021; F. Pecora et al. 2022; V. K. Jagarlamudi et al. 2023).

2.2. Detection of Alfvénic Fluctuations

We identify Alfvén fluctuations using the method proposed by H. Li et al. (2016), which employs bandpass-filtered plasma velocity and magnetic field observations. This approach minimizes the uncertainties of determining the background magnetic field and the de Hoffmann–Teller frame. The quality of Alfvénicity is evaluated using the parameter E_{rr}, defined as the mean of eight parameters: (1) $||\gamma_c| - 1|$; (2) $||\gamma_{cx}| - 1|$; (3) $||\gamma_{cy}| - 1|$; (4) $||\gamma_{cz}| - 1|$; (5) $|\sigma_{\delta V}/\sigma_{\delta V_A} - 1|$; (6) $|\sigma_{\delta V_x}/\sigma_{\delta V_{Ax}} - 1|$; (7) $|\sigma_{\delta V_y}/\sigma_{\delta V_{Ay}} - 1|$; and (8) $|\sigma_{\delta V_z}/\sigma_{\delta V_{Az}} - 1|$. Here, γ_c denotes the correlation coefficient between the fluctuations (δ) of plasma velocity (V) and Alfvén velocity (V_A), while σ represents the standard deviation.

Following previous studies such as H. Li et al. (2016, 2020), we select 10 logarithmic frequency bands with equal spacing: 10–15, 15–25, 25–40, 40–60, 60–100, 100–160, 160–250, 250–400, 400–630, and 630–1000 s. The fragments with $E_{rr} < 0.3$ for three or more filters are marked as Alfvén waves. Based on this, we can define the Alfvén wave fraction within a time period as

$$f_{\rm AW} = \frac{T_{\rm AW}}{T_{\rm total}} \times 100\%, \tag{2}$$

where $T_{\rm AW}$ is the duration marked as Alfvén waves within the time period, and $T_{\rm total}$ is the total duration of the time period. And the purity of the Alfvén wave in the segments is denoted by the average E_{rr} values from the five lower-frequency channels.

Additionally, we estimate the growth rate of parametric decay instability (PDI), which can weaken Alfvén waves (A. Galeev & V. Oraevskii 1963; R. Z. Sagdeev & A. A. Galeev 1969; N. F. Derby 1978; M. L. Goldstein 1978). The instability growth rate is given by

$$\gamma/\omega_0 = \frac{1}{2\sqrt{2}\,\beta^{1/4}}\delta B/B_0, \tag{3}$$

where ω_0 is the angular frequency of the mother wave, B_0 is the background magnetic field (frequency range : 0–1/2000 Hz), and δB is the magnetic field fluctuation.

3. Results

3.1. Switchbacks Associated with High-speed Stream

Figure 1 shows the occurrence of switchbacks and the Alfvénicity of the solar wind over a 5 day period before and after a high-speed stream. We present the occurrence rate per unit distance rather than per unit time to eliminate the influence of solar wind speed on the switchback occurrence rate. The figure shows that the spatial distribution of switchbacks closely correlates with regions of high Alfvénicity, with sporadic high Alfvénicity regions corresponding to sporadic switchback events. Given that high-speed solar wind generally exhibits stronger Alfvénicity, this relationship is also evident when considering solar wind speed on larger timescales.

3.2. Plasma Conditions during Switchbacks

To address two fundamental questions, as follows, we compare the plasma conditions during switchbacks with those of the surrounding solar wind: Does the Alfvénicity during a switchback show a significant difference from the surrounding

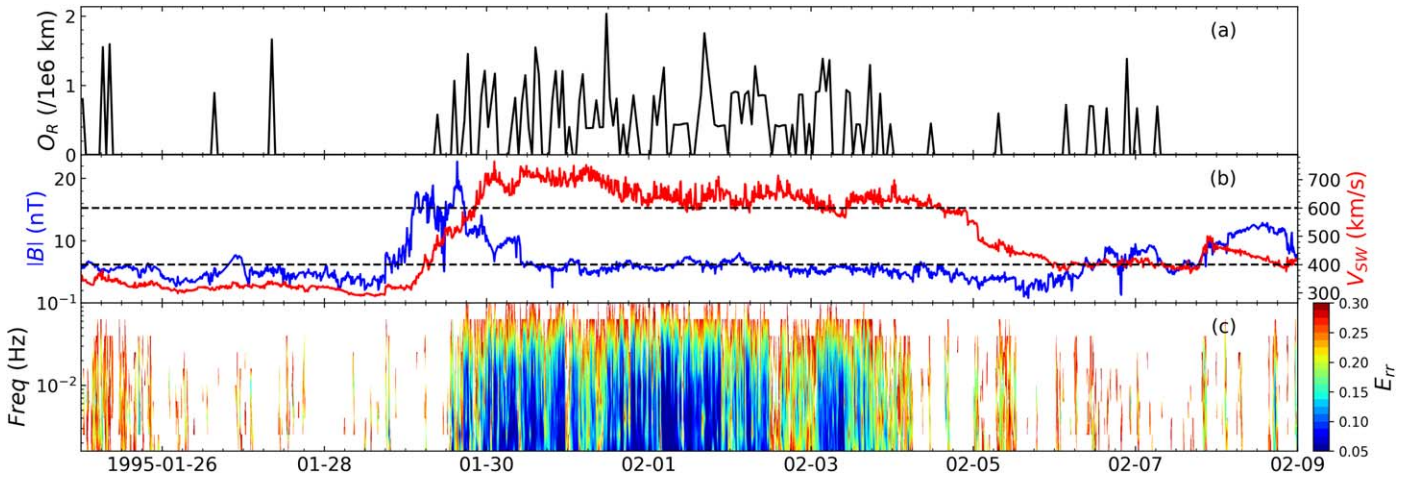

Figure 1. Overview of switchbacks identified before and after a high-speed stream. (a) Switchback occurrence rate per unit distance, O_R. (b) Magnetic field intensity, $|B|$ (blue), and solar wind speed, $|V_{SW}|$ (red). (c) Time-frequency distribution of E_{rr}.

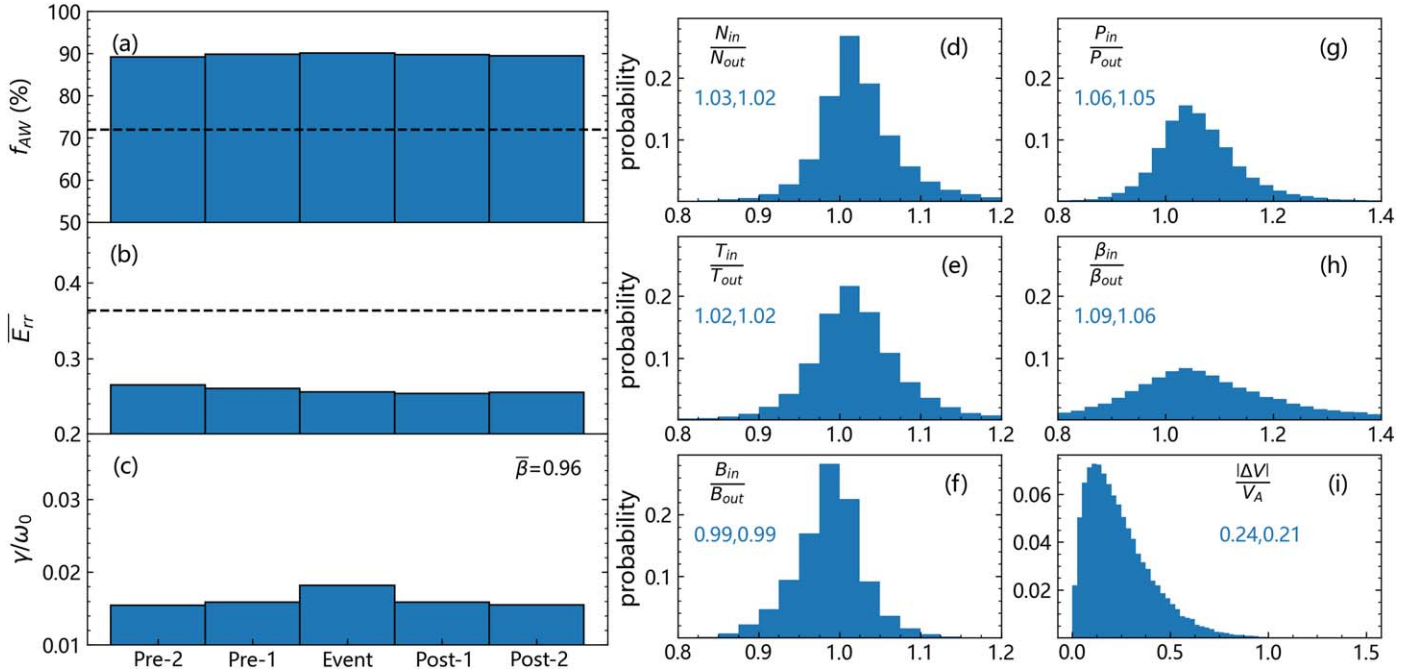

Figure 2. Comparison of Alfvénicity and plasma parameters of the switchback with the surrounding solar wind. (a)–(c) The ratio of Alfvén wave fraction f_{AW}, Alfvén wave purity $\overline{E_{rr}}$, and the average instability growth rate of parameters γ/ω_0 for switchback compared to the surrounding solar wind before and after the switchback. The horizontal axis represents five time intervals: Pre-2 (two intervals before the event), Pre-1 (one interval before the event), Event (the switchback interval itself), Post-1 (one interval after the event), and Post-2 (two intervals after the event). The black dashed line represents the average level of the entire solar wind. (d)–(h) The distribution of ratios of the average value measured during the switchback to that measured in the surrounding solar wind, for proton density, proton temperature, magnetic field strength, total pressure, and plasma β, respectively. (i) The distribution of the relative shear speed of the solar wind during the switchbacks. The two values on the left side of each subplot represent the mean and the median, respectively.

solar wind? Is there a strong velocity shear between the switchback and the surrounding solar wind?

Figure 2 presents the Alfvénicity and plasma parameters of switchbacks and the surrounding solar wind. Figure 2(a) shows that the average Alfvén wave fraction during switchbacks is comparable to those in the surrounding solar wind, with values of 90.1% and 89.6%, respectively, both significantly higher than the overall solar wind level of 72.0%. The result of the average Alfvén wave purity shown in Figure 2(b), denoted by E_{rr}, is similar. The E_{rr} values are 0.256 and 0.259 during switchbacks and in the surrounding solar wind, respectively, significantly less than the overall solar wind level of 0.363. A smaller E_{rr} value indicates stronger Alfvénicity. Figure 2(c) shows that the growth rate of PDI slightly increases during switchbacks but remains at a relatively low level. The average plasma β during switchbacks is 0.96, consistent with previous studies suggesting that plasma β values close to 1 are favorable for switchback formation (J. Squire et al. 2020). Under such conditions, Alfvén waves do not exhibit significant damping even when the growth rate of PDI slightly increases (H. Li et al. 2020). This implies that switchbacks do not lead to local Alfvén wave dissipation.

Figure 2(d)–(f) shows minor differences between switchbacks and the surrounding plasma conditions, presenting a normal distribution with a mean ratio close to 1 and less than 10% variations in proton density, proton temperature, and

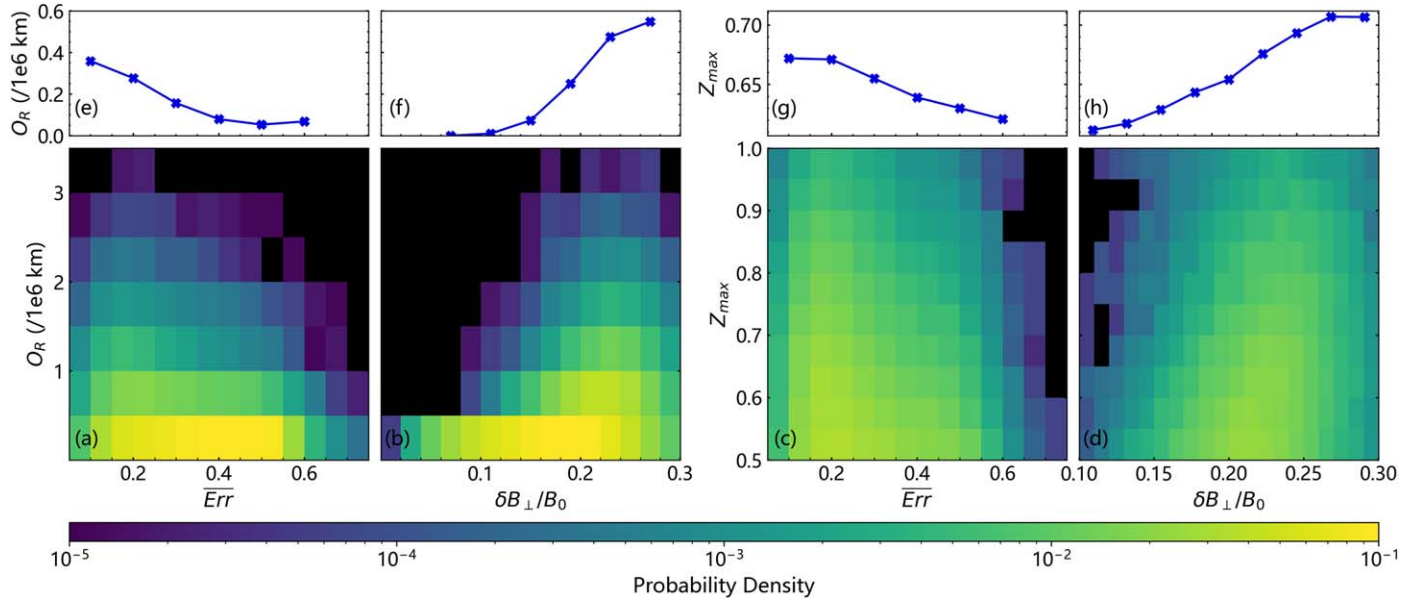

Figure 3. (a) Distribution of switchback occurrence rate with Alfvén wave purity. (b) Distribution of switchback occurrence rate with Alfvén wave amplitude during hours when the average Alfvén wave purity is less than 0.3. (c) and (d) are the same format as (a) and (b), but with occurrence rate replaced by maximum deflection degree. (e)–(h) are the corresponding marginal probability distributions.

magnetic field strength. Figure 2(g) shows that the total pressure inside the switchbacks is mostly (81%) larger than that of the surrounding solar wind, with a mean ratio of 1.06, indicating an expansion of switchbacks during their propagation in the solar wind. Figure 2(h) shows the result for plasma β, similar to the total pressure, with a larger mean ratio of 1.09 and a larger expansion in distribution. Figure 2(i) indicates that the average ratio of the absolute value of the solar wind shear speed to the Alfvén speed is 0.24, with very few events exceeding a ratio of 1. According to D. Ruffolo et al. (2020), switchbacks are generated by instabilities only when the velocity shear exceeds the Alfvén speed. However, our results indicate that the switchbacks we focused on might not be generated by the velocity shear mechanism. As approximated by Y. D. Liu et al. (2023), if switchbacks are Alfvénic fluctuations, the shear speed is at most $|\Delta V| = V_A \cdot 2 \cdot \bar{z}$, where $\bar{z}$ represents the averaged value of z during the switchback. In our study, 99.5% of the events satisfy this condition.

3.3. Occurrence Rate and Deflection Degree of Switchbacks

Previous studies on occurrence rates have primarily focused on their evolution with heliocentric distance, yielding varying results due to differences in satellite observations and periods (A. R. Macneil et al. 2020; F. S. Mozer et al. 2021; A. Tenerani et al. 2021; F. Pecora et al. 2022; V. K. Jagarlamudi et al. 2023). One possible reason for these discrepancies is the variation in solar wind conditions at the same heliocentric distance during different periods. To address this, we investigate the impact of solar wind conditions at 1 au on the occurrence rate and deflection degree of switchbacks.

Figure 3 shows the relationship between large amplitude Alfvén waves and the occurrence rate and deflection degree of switchbacks in a 1 hr window. The amplitude, $\delta B_\perp/B_0$, is defined as the ratio of the standard deviation of the perpendicular magnetic field component to the background magnetic field, considering only hours with an average Alfvén wave purity ($\overline{E_{rr}}$) less than 0.3. Figures 3(a) and (c) reveal that higher switchback occurrence rates are more frequently observed during intervals with stronger Alfvénicity, and the maximum deflection degree of switchbacks is also greater during these periods. Figures 3(b) and (d) further demonstrate that the intervals with high occurrence rates and large maximum deflection degrees correspond to the portions of Alfvén wave segments with larger amplitudes, which is a natural result.

Figure 4 examines the relationship between switchback occurrence rate and solar wind speed. Figures 4(a) and (b) show that at 1 au, higher solar wind speeds are associated with higher Alfvénicity, while within 0.25 au, Alfvénicity remains high regardless of speed. Figure 4(c) reveals a clear positive correlation between switchback occurrence rate and solar wind speed at 1 au, while within 0.25 au, the occurrence rate only shows a slight increase with solar wind speed. However, considering only periods with large amplitude Alfvén waves, this correlation disappears. Under that situation, the occurrence rate remains nearly constant.

We studied 48 high-speed streams and their surrounding regions from the event list provided by J. E. Borovsky (2016), where the WIND spacecraft's position met our research requirements and had complete data. The selected high-speed streams exhibit a "flattop-like" shape in their solar wind velocity profiles. Figure 5 characterizes the Alfvénicity of the solar wind (including Alfvén wave fraction and purity) and the occurrence rate and maximum deflection of switchbacks in these streams and their surrounding regions. The results show that the occurrence rate and deflection degree of switchbacks are highest in the high-speed stream region, followed by the leading and trailing edges, and then the upstream and downstream. This pattern aligns with the variations in Alfvénicity of the corresponding solar wind in these regions. According to Y. D. Liu et al. (2023), the transition regions on both sides of high-speed streams are characterized by strong velocity shear and are likely regions where the footpoints of magnetic field lines switch between slow and fast solar wind

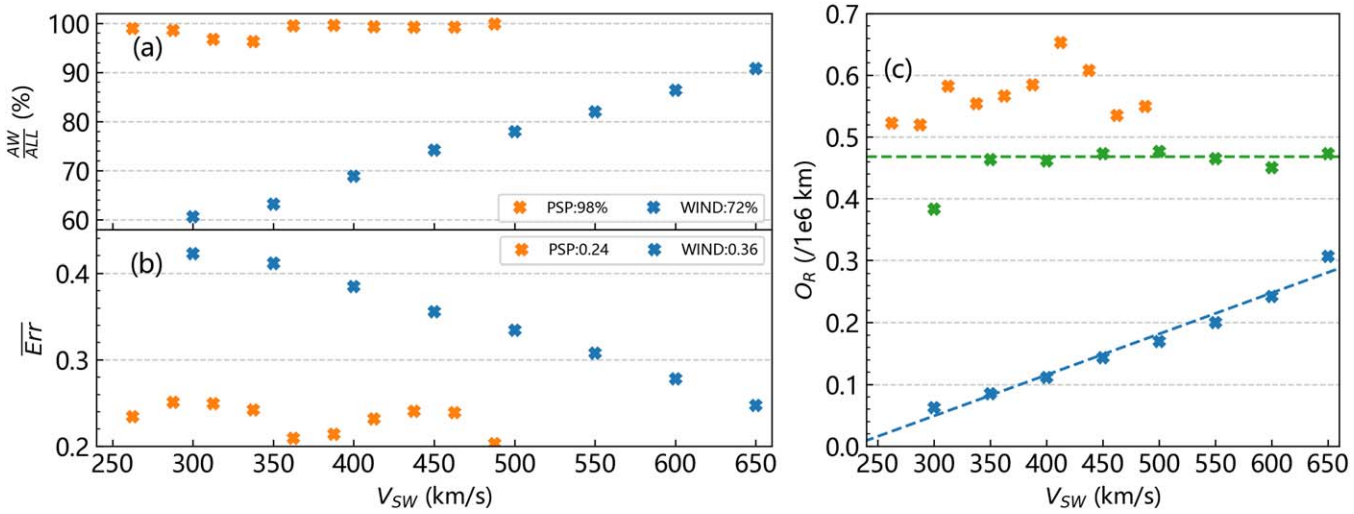

Figure 4. (a) and (b) show the proportions and purity of Alfvén waves in the solar wind at different speeds. PSP data (orange) covers the period from 2018-11-01 to 2018-11-11. (c) Relationship between switchback occurrence rate and solar wind speed. PSP data (orange) are from the first 17 encounters (heliocentric distances less than 0.25 au), while WIND data (blue) cover the entire time. Green indicates period with large-amplitude Alfvén waves ($\overline{\mathrm{Err}} < 0.3$ and $\delta B_\perp/B_0 > 0.2$).

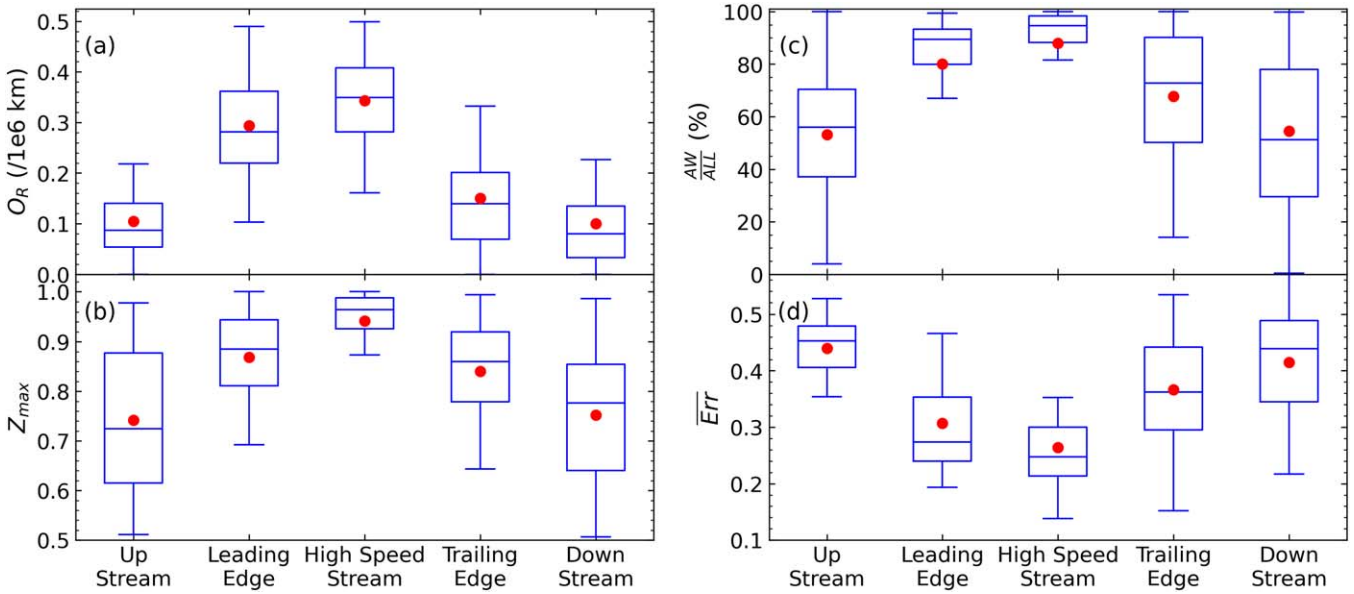

Figure 5. The high-speed stream and its surrounding regions (leading edge, trailing edge, upstream, and downstream): (a) switchback occurrence rate, (b) maximum deflection angle of switchbacks, (c) Alfvén wave contribution, and (d) Alfvén wave purity. Here, upstream and downstream correspond to 1 day outside the leading edge and trailing edge, respectively.

sources. However, our results indicate that the occurrence rate and deflection degree of switchbacks are not significantly influenced by velocity shear or footpoint motion.

4. Discussion

We analyzed the differences in plasma conditions between switchbacks and their surrounding environment, shown in Figure 2. Both switchbacks and the surrounding solar wind exhibit high Alfvénicity, with velocity disturbances consistent with the characteristics of Alfvén waves. This indicates that switchbacks are structures embedded within high-purity Alfvénic solar wind.

We examined the relationship between the occurrence rate and maximum deflection of switchbacks and the Alfvén wave purity and amplitude within a specified time interval, as shown in Figure 3. The results indicate that under large amplitude Alfvén waves, the occurrence rate and maximum deflection of switchbacks increase significantly. This finding, together with the observation that the correlation between switchback occurrence rate and solar wind speed vanishes when restricted to periods of large-amplitude Alfvén waves (Figure 4), indicates that the increase in switchback occurrence rate with increasing solar wind speed is primarily driven by the enhanced Alfvénicity within the solar wind.

We compared the high-speed stream and its surrounding regions in Figure 5 and found that the transition regions, which are considered to have stronger velocity shear and are more prone to footpoint motion, did not exhibit higher switchback

occurrence rates or greater maximum deflection angles. This suggests that these two mechanisms (D. Ruffolo et al. 2020; N. Schwadron & D. McComas 2021; G. Toth et al. 2023) are not the dominant factors in the formation of switchbacks.

Switchbacks observed by PSP in the inner heliosphere typically exhibit nearly incompressible characteristics (S. Bale et al. 2019; J. C. Kasper et al. 2019), which are not naturally satisfied at greater distances from the Sun and should be explicitly constrained in studies, as done by A. Tenerani et al. (2021) and T. S. Horbury et al. (2023). We examined the statistical characteristics of compressible events with $C_{\rm SB} \geqslant 0.1$ that were excluded in the previous sections, the main differences are as follows:

1. Lower Alfvénicity compared to the surrounding environment, higher plasma beta (5 times), and higher PDI growth rate (2 times).
2. Significant reduction in the total magnetic field, with more scattered variations in plasma beta.
3. A positive correlation between the occurrence and PDI growth rates.

These "excluded potential switchbacks" account for 37% of all "potential switchbacks." Given the notable differences mentioned above, we speculate that these events may result from the increased growth rate of parametric instability under higher beta conditions, which leads to the attenuation of Alfvén waves while simultaneously generating compressive fluctuations (M. Shi et al. 2015; H. Li et al. 2020). According to the research by M. Marriott & A. Tenerani (2024a, 2024b), the coupling with compressible and Alfvénic modes due to parametric instability may be responsible for the decay of switchbacks; these excluded events could potentially be remnants of switchbacks decaying under conditions of increased parametric instability growth rates.

We investigated the occurrence rate of switchbacks using multiple time windows, ranging from 1 hr to 1 day, and calculated their correlation coefficients with four parameters: the solar wind speed $V_{\rm SW}$, Alfvén wave purity $\overline{E_{rr}}$, the growth rate of PDI γ/ω_0, and velocity shear $\Delta V/V_{\rm SW}$. Two key features suggest that switchbacks are more likely to occur in clustered regions of Alfvén waves rather than in isolated, small Alfvén wave segments:

1. The occurrence rate of switchbacks is notably higher in Alfvén wave segments with longer durations.
2. The correlation with $\overline{E_{rr}}$ is consistently the strongest and becomes increasingly significant, reaching a value of -0.65 as the window length increases. In contrast, the correlation with $\Delta V/V_{\rm SW}$ progressively diminishes, decreasing from 0.22 to nearly zero.

5. Summary

This study investigates the relationship between switchbacks and solar wind conditions, particularly focusing on the role of Alfvén waves in the formation and characteristics of switchbacks. Our main findings are summarized as follows:

1. *Concentration of switchbacks in Alfvén waves.* Switchbacks are predominantly found during periods of Alfvén waves. The occurrence rate and maximum deflection of switchbacks are positively correlated with the purity and amplitude of Alfvén waves. This suggests that Alfvén waves play a crucial role in the formation and enhancement of switchbacks.
2. *Independence from solar wind speed.* During periods of high-amplitude Alfvén waves, the occurrence rate of switchbacks per unit distance shows no significant correlation with solar wind speed. This indicates that the switchbacks are embedded within Alfvén waves, and the increase in switchback occurrence rate with increasing solar wind speed is primarily driven by the enhanced Alfvénicity within the solar wind, rather than by solar wind speed itself.
3. *Suitability of large time windows.* Our analysis suggests that switchbacks are more effectively studied using large time windows. This is because switchbacks tend to occur in clustered regions of Alfvén waves rather than in isolated small Alfvén wave segments. Longer time windows capture these clustered events more accurately.
4. *Impact of magnetic compression.* Potential switchbacks excluded due to strong magnetic compression (characterized by $C_{\rm SB} \geqslant 0.1$) are likely the result of Alfvén wave dissipation caused by PDI. These events exhibit lower Alfvén wave fraction and purity, higher plasma β, and increased growth rates of PDI compared to typical switchbacks.

In conclusion, based on our findings, it can be speculated that switchbacks represent the extreme-large-amplitude tail of the distribution of Alfvén wave amplitudes, which is consistent with the theory that Alfvén waves in the expanding solar wind can naturally develop into switchbacks (J. Squire et al. 2020; A. Mallet et al. 2021; M. Shoda et al. 2021; Z. Johnston et al. 2022; J. Squire et al. 2022). However, whether these large-amplitude Alfvén waves are locally generated or propagated from the corona cannot be determined in this study. Therefore, the possibilities of a coronal origin for switchbacks, e.g., interchange reconnection (L. Fisk & J. Kasper 2020; G. Zank et al. 2020; J. Drake et al. 2021; S. Bale et al. 2023) and coronal jets (A. C. Sterling & R. L. Moore 2020) cannot be ruled out. Future studies are needed to clarify this issue. Understanding the evolution and dynamics of Alfvén waves in the solar wind is essential for a comprehensive understanding of switchbacks. Future research should focus on further exploring the mechanisms underlying the interaction between Alfvén waves and switchbacks, as well as the conditions that lead to Alfvén wave dissipation and the formation of switchbacks.

Acknowledgments

The authors thank NASA CDAWEB (https://cdaweb.gsfc.nasa.gov/index.html) for providing the WIND and PSP data. This work is supported by NNSFC grants (42374198 and 42188101), the project of Civil Aerospace "14th Five Year Plan" Preliminary Research in Space Science (D010202 and D010301). H.L. is also supported by the China-Brazil Joint Laboratory for Space Weather (No. 119GJHZ2024027MI).

ORCID iDs

Hui Li https://orcid.org/0000-0002-4839-4614
Fanzhuo Dai https://orcid.org/0009-0009-8460-9609
Chi Wang https://orcid.org/0000-0001-6991-9398
Wence Jiang https://orcid.org/0000-0001-7431-5759

References

Bale, S., Badman, S., Bonnell, J., et al. 2019, Natur, 576, 237
Bale, S., Drake, J., McManus, M., et al. 2023, Natur, 618, 252
Borovsky, J. E. 2016, JGRA, 121, 5055
Cheng, W., Liu, Y. D., Ran, H., et al. 2024, ApJ, 967, 58
Derby, N. F., Jr 1978, ApJ, 224, 1013
Drake, J., Agapitov, O., Swisdak, M., et al. 2021, A&A, 650, A2
Dudok de Wit, T., Krasnoselskikh, V. V., Bale, S. D., et al. 2020, ApJS, 246, 39
Fisk, L., & Kasper, J. 2020, ApJL, 894, L4
Galeev, A., & Oraevskii, V. 1963, SPhD, 7, 988
Goldstein, M. L. 1978, ApJ, 219, 700
Horbury, T. S., Bale, S. D., McManus, M. D., et al. 2023, PhPl, 30, 082905
Horbury, T. S., Matteini, L., & Stansby, D. 2018, MNRAS, 478, 1980
Huang, N., D'Anna, S., Wang, H., et al. 2023, ApJL, 946, L17
Jagarlamudi, V. K., Raouafi, N., Bourouaine, S., et al. 2023, ApJL, 950, L7
Johnston, Z., Squire, J., Mallet, A., & Meyrand, R. 2022, PhPl, 29, 129902
Kasper, J. C., Bale, S. D., Belcher, J. W., et al. 2019, Natur, 576, 228
Lepping, R., Acũna, M., Burlaga, L., et al. 1995, SSRv, 71, 207
Li, H., Li, N., Wang, C., & Yao, S. 2020, ApJL, 889, L16
Li, H., Wang, C., Chao, J., & Hsieh, W. 2016, JGRA, 121, 42
Lin, R., Anderson, K., Ashford, S., et al. 1995, SSRv, 71, 125
Liu, Y. D., Ran, H., Hu, H., & Bale, S. D. 2023, ApJ, 944, 116
Macneil, A. R., Owens, M. J., Wicks, R. T., et al. 2020, MNRAS, 494, 3642
Mallet, A., Squire, J., Chandran, B. D., Bowen, T., & Bale, S. D. 2021, ApJ, 918, 62
Marriott, M., & Tenerani, A. 2024a, ApJ, 967, 19
Marriott, M., & Tenerani, A. 2024b, ApJ, 975, 232
Mozer, F. S., Bale, S., Bonnell, J., et al. 2021, ApJ, 919, 60
Pecora, F., Matthaeus, W. H., Primavera, L., et al. 2022, ApJL, 929, L10
Ruffolo, D., Matthaeus, W. H., Chhiber, R., et al. 2020, ApJ, 902, 94
Sagdeev, R. Z., & Galeev, A. A. 1969, Nonlinear Plasma Theory (New York: Benjamin)
Schwadron, N., & McComas, D. 2021, ApJ, 909, 95
Shi, M., Xiao, C., Li, Q., et al. 2015, ApJ, 815, 122
Shoda, M., Chandran, B. D., & Cranmer, S. R. 2021, ApJ, 915, 52
Squire, J., Chandran, B. D., & Meyrand, R. 2020, ApJL, 891, L2
Squire, J., Johnston, Z., Mallet, A., & Meyrand, R. 2022, PhPl, 29, 112903
Sterling, A. C., & Moore, R. L. 2020, ApJL, 896, L18
Tenerani, A., Sioulas, N., Matteini, L., et al. 2021, ApJL, 919, L31
Toth, G., Velli, M., & van der Holst, B. 2023, ApJ, 957, 95
Yamauchi, Y., Suess, S. T., Steinberg, J. T., & Sakurai, T. 2004, JGRA, 109, A03104
Zank, G., Nakanotani, M., Zhao, L.-L., Adhikari, L., & Kasper, J. 2020, ApJ, 903, 1